gels

MDPI

Article

Catalytic Reduction of Environmental Pollutants with Biopolymer Hydrogel Cross-Linked Gelatin Conjugated Tin-Doped Gadolinium Oxide Nanocomposites

Hadi M. Marwani [1,2], Shahid Ahmad [1] and Mohammed M. Rahman [1,2,*]

[1] Department of Chemistry, Faculty of Science, King Abdulaziz University, P.O. Box 80203, Jeddah 21589, Saudi Arabia; hmarwani@kau.edu.sa (H.M.M.); drchemsci@gmail.com (S.A.)
[2] Center of Excellence for Advanced Materials Research (CEAMR), King Abdulaziz University, P.O. Box 80203, Jeddah 21589, Saudi Arabia
* Correspondence: mmrahman@kau.edu.sa; Tel.: +966-12-695-2293; Fax: +966-12-695-2292

Abstract: In the present study, a biopolymer nanocomposite hydrogel based on gelatin and tin-doped gadolinium oxide (Sn-Gd_2O_3@GH) was prepared for the efficient reduction of water pollutants. The method of Sn-Gd_2O_3@GH preparation consisted of two steps. A Sn-Gd_2O_3 nanomaterial was synthesized by a hydrothermal method and mixed with a hot aqueous solution (T > 60 °C) of gelatin polymer, followed by cross-linking. Due to the presence of abundant functional groups on the skeleton of gelatin, such as carboxylic acid (–COOH) and hydroxyl (–OH), it was easily cross-linked with formaldehyde. The structure, morphology, and composition of Sn-Gd_2O_3@GH were further characterized by the FESEM, XRD, EDX, and FTIR techniques. The FESEM images located the distribution of the Sn-Gd_2O_3 nanomaterial in a GH matrix of 30.06 nm. The XRD patterns confirmed the cubic crystalline structure of Gd_2O_3 in a nanocomposite hydrogel, while EDS elucidated the elemental composition of pure Sn-Gd_2O_3 powder and cross-linked the Sn-Gd_2O_3@GH samples. The synthesized Sn-Gd_2O_3@GH nanocomposite was used for the removal of different azo dyes and nitrophenols (NPs). It exhibited an efficient catalytic reduction of Congo red (CR) with a reaction rate of 9.15×10^{-1} min^{-1} with a strong $NaBH_4$-reducing agent. Moreover, the Sn-Gd_2O_3@GH could be easily recovered by discharging the reduced (colourless) dye, and it could be reused for a fresh cycle.

Keywords: gelatin hydrogel; Sn-Gd_2O_3@GH; nanocomposite; catalytic reduction; nitrophenols; azo dye

Citation: Marwani, H.M.; Ahmad, S.; Rahman, M.M. Catalytic Reduction of Environmental Pollutants with Biopolymer Hydrogel Cross-Linked Gelatin Conjugated Tin-Doped Gadolinium Oxide Nanocomposites. *Gels* **2022**, *8*, 86. https://doi.org/10.3390/gels8020086

Academic Editor: Bjørn Torger Stokke

Received: 9 December 2021
Accepted: 21 January 2022
Published: 28 January 2022

1. Introduction

The presence of a low concentration of synthetic dyes is a serious threat to the reuse of industrial wastewater. Natural water sources are contaminated by heavy metals and hazardous dyes, such as nitrophenols, azo dyes, phthalates, and herbicides, with most contributions coming from oil refining and industrial discharges [1–3]. Dyes are mainly used in the textile, painting, leather, printing, and photography industries, among others. These dyes, after completing the dyeing process, are released as effluent to nearby water streams. The presence of these dyes creates environmental problems [4]. In particular, azo dyes contain a nitrogen–nitrogen double bond (–N=N–) and are usually applied in various industries. Various methods have been tried to remove these dyes, such as physical, chemical, and biological methods, electrochemical methods, catalysis, and adsorption [5]. Adsorption is well reported to aid in dye reduction.

Metals and their oxide nanoparticles have played the vital role of catalyst in numerous studies [6–9]. While noble metal nanoparticles have been recognized as the best catalysts for various reactions and sensing applications [10–13], their high cost limits their applications on a large scale. In contrast to noble metals, other transition metal nanoparticles, such as tin, copper, nickel, iron, and cobalt, have been reported [6–8,10–12,14–22] to show

enhanced catalytic properties, but their stability is a major problem faced in such studies. On the other hand, transition metal oxides are quite stable in aqueous environments, and some studies have reported their use as catalysts for the degradation of dyes by electron transfer reaction [23–28]. Copper oxide, zinc oxide, ferric oxide, tin oxide, and pure metal nanoparticles could be used as catalysts, but their aggregation and separation after the reaction is complete are the main problems. Different supporting surfaces, such as block types, magnetic nanoparticles, copolymer micelles, polymer sheets, and latex particles have been used for stabilizing and easy separation [6,10,29–31]. Polymer hydrogels are considered to be the best for supporting catalytic nanoparticles [31]. Hydrogels are defined as cross-linked, polymeric matrix, water-swollen materials, and hydrophilic three -dimensional polymeric hydrogels have the capacity to absorb a huge amount of water and retain it without dissolution [29,31,32]. They are widely used in smart materials for controlled drug delivery, catheter coatings, tissue engineering, food chemistry, and wastewater treatment [30,33–35].

Rare earth elements were discovered in 1788. They consist of seventeen (17) metallic elements. In today's society, REEs are widely used in metallurgy, high technology, military defense systems, clean energy, medical fields, fluid and auto-catalysis, wind-power turbines, electric vehicles, energy-efficient lighting, and catalytic converters [36,37]. REEs are a vital part of more than 200 products globally and many high-tech devices. Rare earth oxides (RE_2O_3) are most stable in their trivalent form due to their physical, electronic, and chemical properties resulting from the 4f orbital [38].

Gadolinium is a trivalent metal discovered by Johan Gadolin. Its oxide (Gd_2O_3) has drawn attention in the fields of garnets, magnetic resonance imaging relaxation, alloys, neutron capture, and lasers [39]. The oxide is white, odourless, and not soluble in water but soluble in acids. The oxide exists in three different forms—hexagonal (h-Gd_2O_3), monoclinic (m-Gd_2O_3), and cubic (c-Gd_2O_3). As a catalyst, it is used as a neutron converter in imaging plate neutron detectors, as an additive in uranium oxide (UO_2) fuel rods and ceramics such as SiC, Si_3N_4, and ZrO_2, and as a dimerization catalyst for organic compounds [40]. For the preparation of metal oxide NPs, surfactants play a vital role due to their effects on coagulation, flocculation, and particle growth [41]. Several other methods have been used for metal oxide synthesis, such as the precipitation method, the ultrasonic method, two-step solid-state reaction, spray pyrolysis, the sol-gel process, surfactant-mediated, and the hydrothermal method [42,43].

The hydrophilicity and cross-linking of polymeric chains play a vital role in investigating the properties of hydrogels and other materials. The swelling ability of hydrogels is mainly related to the hydrophilic functional group, such as carboxylic, amino acid, hydroxyl, and primary amidic, that is present in the backbone of the polymer main chain [44]. The cross-linking of this functional group between the chains makes hydrogels insoluble in water. On the basis of their swelling ability, hydrogels are categorized according to pore size. Hydrogels can be categorized as (a) non-porous, (b) micro-porous, or (c) super-porous. In non-porous hydrogels, swelling occurs through diffusion only. Micro-porous hydrogels contain pores from a few microns to several 100 micros in size, in which swelling results through diffusion as well as leaching. Super-porous hydrogels contain large-sized pores, which speed up swelling rates and, hence, cause massive swelling [45]. One serious disadvantage of such matrices is the thermal and structural lability, which can be improved with cross-linkers, such as formaldehyde [46] and glutaraldehyde [47]. In addition to their stability, hydrogels also alter swelling and, thus, trap the material inside for a longer time [48].

Therefore, biopolymers such as gelatin, chitosan, and silk proteins are widely used for hydrogel fabrications due to their essential biocompatible nature [49–51]. Among these polymers, gelatin has attracted the attention regarding hydrogel synthesis, due to the presence of large number of metal-binding sites on its chains [52,53]. It synthesizes industrially, playing an important role in food, photographic, and pharmaceutical industries [54]. The major sources include pig skin (46%), bovine hides (collagen) (29.4%), and cattle bones

(23.1%). Gelatin composition is almost similar to collagen. Changes in its structure emerge during its manufacturing process. On heating, the collagen are transferred into helixes which, upon cooling, partly regain structure, are converted into gelatin containing water, and form gel. However, due to its brittle and fragile network, it is limited in application. To control these limitations, MNPs have been introduced to form hydrogel nanocomposites [55]. The entrapped NPs either cross-link the chains of the hydrogel or absorb on the polymer chain, forming a three-dimensional network [56]. These networks are resulted due to covalent and noncovalent bonds through physical or chemical interactions. The MNPs and polymer work together to produce unique properties, such as thermal, mechanical, and optical, which leads the hydrogel nanocomposites to be used in sensors, catalysts, electronics, optics, and in separation devices [57]. Gelatin hydrogel can also be used as biodegradable material in the pharmaceutical and medical industries [56,58,59]. Moreover, it can be cross-linked easily due to the presence of a large number of functional groups [60].

Therefore, herein, the gelatin hydrogel nanocomposite was prepared by the incorporation of gadolinium doped tin dioxide nanomaterials and cross-linked with formaldehyde. The prepared hydrogel nanocomposite was studied as a catalyst for the reduction of different environmental pollutants. Additionally, the prepared hydrogel exhibits low cost, highly efficiency for the removal of dyes, potential recyclability, and easy separation.

2. Experimental

2.1. Materials

The chemicals and reagents used this experiment were analytical grade. Gelatin ($C_{102}H_{151}O_{39}N_{31}$), 4-nirophenol (4-NP–$C_6H_5NO_3$), 2-nitrophenol (2-NP–$C_6H_5NO_3$), 2,6-dinitrophenol (2,6-DNP–$C_6H_4N_2O_5$), and methylene blue (MB; $C_{16}H_{18}ClN_3S$) were purchased from Fluka, UK. Aridine orange (ArO; $C_{17}H_{19}N_3$), congo red (CR-$C_{32}H_{22}N_6Na_2O_6S_2$), and methyl orange (MO; $C_{14}H_{14}N_3NaO_3S$) were purchased from Sigma-Aldrich chemical company (Austin, TX, USA). Reducing agent, sodium borohydride ($NaBH_4$, 97%), was purchased from BDH chemicals, Poole, United Kingdom. Ultra-pure distilled water was used for the preparation of all the solutions. The molecular structure of all target chemicals and dyes such as 2-NP, 4-NP, 2,6-DNP, MB, MO, and CR are given in Scheme 1.

2.2. Synthesis of Sn-Gd_2O_3 Nanomaterial

Gadolinium is a vital substance for doping due to its chemical stability. Here, a one-step way of fabrication is followed for Sn-Gd_2O_3 nanomaterial. In the first step, 0.1 M solution of gadolinium salt [$Gd(NO_3)_3{\cdot}6H_2O$] was prepared, dissolving 2.26 gm in 50 mL of distilled water. Similarly, 0.01 M solution of $SnCl_4$ salt (0.1303 gm) was freshly prepared in 50 mL of ethanol. The $SnCl_4$ solution was set on vigorous stirring for 1hr, until a colourless solution was obtained. In the second step, both solution [$Gd(NO_3)_3{\cdot}6H_2O$] and $SnCl_4$ was mixed up in 100 mL of round bottom flask. The pH of the final solution was adjusted above 10 by adding drop wise NH_4OH solution. Again, the solution was kept for stirring, forming colloidal suspension, after 1 h. Finally, the solution was transferred to a Teflon-lined autoclave at 150 °C for 3 h, which gives white precipitate. The final product was collected after centrifugation. The resulting white product was washed with water and ethanol and dried at 80 °C overnight.

2.3. Preparation of Gelatin Hydrogel Solution

Gelatin hydrogel was prepared by dissolving of 2.4 gm of gelatin in 30 mL of distilled water, at room temperature. The beaker containing hydrogel was heated mildly at 60 °C, under constant stirring, to prepare a homogenous viscous solution of gelatin polymer.

2.4. Fabrication of Sn-Gd_2O_3@GH Nanocomposite

During adjustments, the 8 wt% concentration of gelatin was found to be good. Thus, 20 mL of gelatin solution was used to prepare hydrogel nanocomposite. The hydrogel was further treated with 4% by weight of Sn doped gadolinium oxide (Sn-Gd_2O_3) in a beaker

under constant stirring for 40 min, to completely homogenize the Sn-Gd_2O_3 nanomaterial. The hydrogel nanocomposite was cross-linked by drained off slowly 5 mL of formaldehyde and left for 24 h to completely cross-link the hydrogel. The prepared solid hydrogel was mashed out and washed three times with distilled water to remove the surplus Sn-Gd_2O_3 NPs (Figure 1).

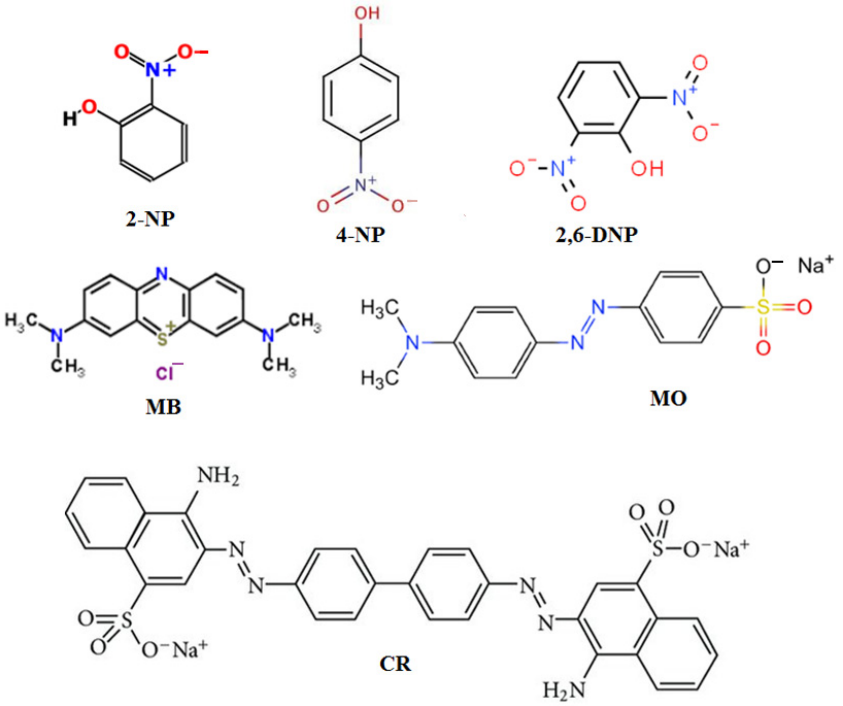

Scheme 1. Molecular structures of 2–NP, 4–NP, 2,6–DNP, MB, MO, and CR.

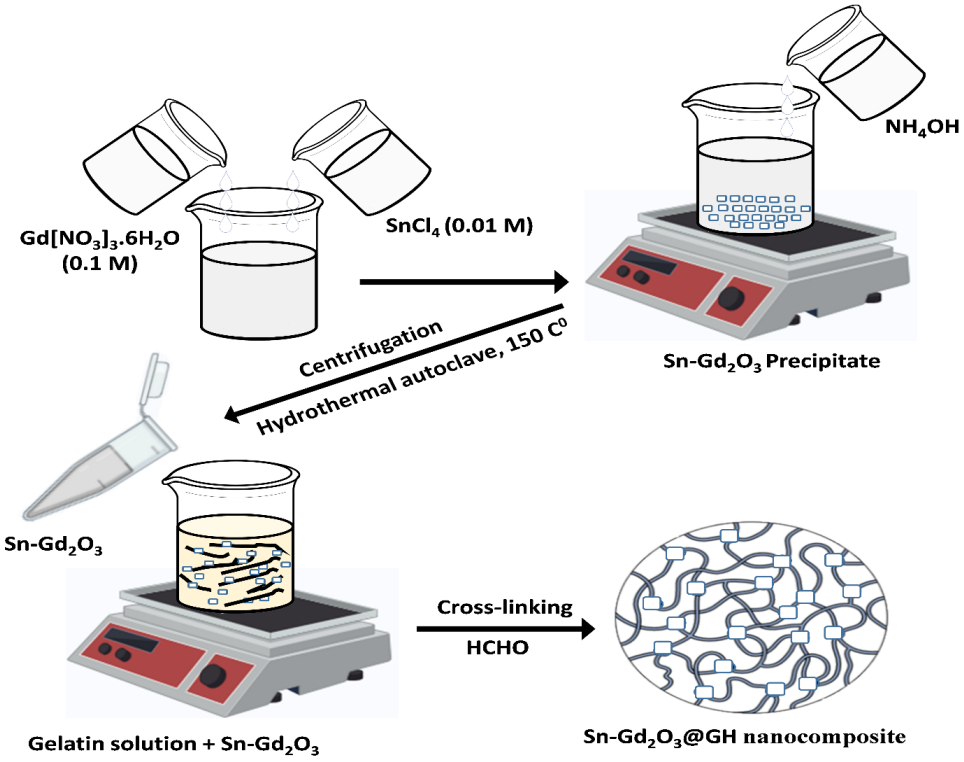

Figure 1. Preparation of Sn-Gd_2O_3@GH nanocomposite.

2.5. Preparation of Dyes Solution

All of the dyes, 4-NP, 2-NP, 2,6-DNP, ArO, MO, and CR, were used. Standard solutions were prepared with desired concentrations of 0.07 mM. Ultra-pure distilled water was used throughout all the experiments.

3. Characterizations

In this approach, scanning electron microscopy, (FESEM) of JEOL, JSM-7600F, Tokyo, Japan, was used for the morphological investigation of Sn-Gd_2O_3@GH nanocomposite, at high accelerating voltage. The prepared sample was coated with platinum before analysis, and attached on 1.5 cm diameter of sticky black tape. The surface elemental composition of the sample was analysed using Oxford energy dispersive X-ray spectroscopy (EDS; Tokyo, Japan) equipment, attached with FESEM (Tokyo, Japan). X-ray diffraction (XRD) experiments were conducted on PANalytical diffractometer using Kα radiation (λ = 0.154 nm) source to investigate the crystallinity of the samples. The voltage of 40 KV and current of 50 mA was set for analysis. The analysis data was recorded in the range of 10° and 80° at a scan rate of 2° 2θ min^{-1}. Fourier transform infrared (FTIR; Berlin, Germany) was used to characterize different functional groups in the Sn-Gd_2O_3@GH nanocomposite hydrogel. The spectra were recorded in the range of 40,000 to 500 cm^{-1} by averaging the 64 scans, using FTIR (Berlin, Germany).

3.1. FESEM Analysis

Field Emission Scanning Electron Microscope (FESEM; Tokyo, Japan) is an electron microscope which is suitable for the analysis of material surface. It is used for observing structures as small as 1 nm. For sample analysis, the primary electrons from a field source are focused and deflected by the lenses which produce a narrow scan beam that investigates the surface morphology of the sample. The secondary electrons are reflected from the material surface to the detectors, which transform it to an electronic signal.

FESEM is used to analyse the surface morphology of the samples, usually for the exterior and cross-sectional area. Figure 2a,b shows the FESEM images of powder Sn-Gd_2O_3 and Sn-Gd_2O_3@GH nano-composite, respectively. The Sn-Gd_2O_3 particles are clearly seen in irregular form as shown in Figure 2a, while, Figure 2b confirms the dispersed nature of Sn-Gd_2O_3 nanomaterials (red circle on SEM image) in the hydrogel matrix. Figure 2b,b′ shows the as synthesized Sn-Gd_2O_3@GH nano-composite present in the white aggregated form. The average particle size of 30.06 nm was calculated. The incorporation of Sn-Gd_2O_3 nanomaterial (red circle on SEM image) changed the morphology of the gelatin polymer; it appeared in grooves and wide roughness, as shown in Figure 2b′.

3.2. EDX Analysis

Energy dispersive-ray spectroscopy is a surface microanalysis characterization to analyse the elemental composition of the sample. Figure 3 elucidates the EDX spectra of Sn-Gd_2O_3 and Sn-Gd_2O_3@GH nanocomposite. EDX spectra showed the existence of Sn, Gd, and O elements into the Sn-Gd_2O_3 doped nano-catalyst (Figure 3a). In another EDX spectrum, it is found the Sn, Gd, O, and C elements into the gelatin polymer coated Sn-Gd_2O_3@GH nanocomposite (Figure 3b). The platinum peak showed due to the platinum coating on the sample. The former EDX spectra for Sn and Gd revealed 26.25 % and 46.86 % by weight, while the second spectra showed 9.46 % and 20.54 % by weight amount of Sn and Gd, respectively. Figure 3b showed the elemental composition of Sn-Gd_2O_3 nanomaterial in the hydrogel matrix. This homogenous distribution confirms the Sn-Gd_2O_3 in the hydrogel nanocomposite.

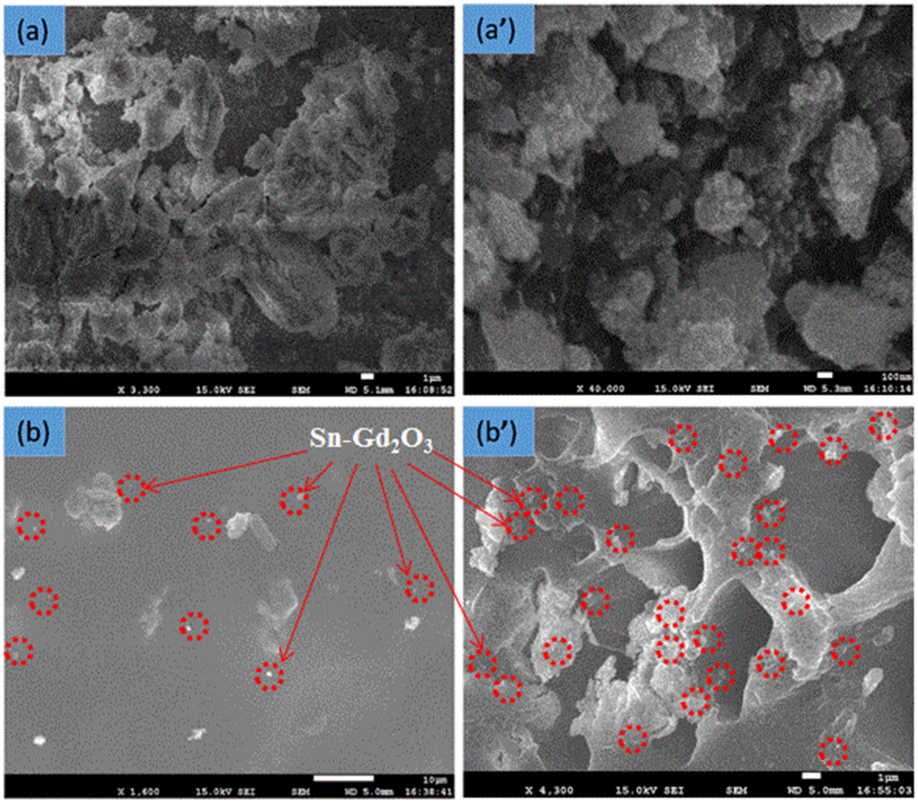

Figure 2. FESEM images of pure Sn-Gd_2O_3 (**a**) and Sn-Gd_2O_3@GH (**b**) at low and their high magnification images (**a′**), (**b′**).

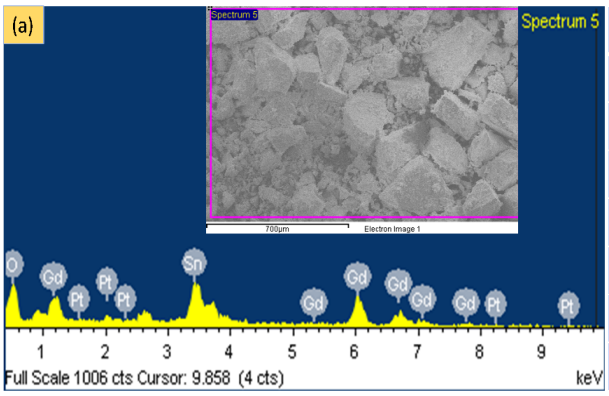

Element	Weight%	Atomic%
C K	25.95	75.00
Sn K	26.25	10.49
Gd K	46.86	14.12
Pt M	1.64	0.40
Total	100.00	

Element	Weight%	Atomic%
C K	49.17	79.48
O K	12.90	15.65
Sn L	9.46	1.55
Gd L	20.54	2.54
Total	100.00	

Figure 3. EDX spectra of Sn-Gd_2O_3 nanomaterial (**a**) and Sn-Gd_2O_3@GH nanocomposite (**b**).

3.3. XRD Analysis

The XRD profiles of powder Sn-Gd_2O_3 nanomaterial and Sn-Gd_2O_3@GH nanocomposite are presented in Figure 4. Figure 4 (Black-line) shows the XRD profile of the Sn-Gd_2O_3 nanomaterial having four sharp peaks. The pattern of Gd_2O_3 powder is exactly coincident with cubic phase Gd_2O_3 (JCPDS card no.12-0797), as published earlier in the related literature [61]. The prominent peaks appeared at 2-theta of 29.39°, 34.12°, 49.12°, and 58.33°, and could be assigned to (222), (400), (440), and (622) diffraction of Sn-Gd_2O_3 nanomaterials, respectively. Figure 4 (Red-line) showed corresponding peaks for Sn-Gd_2O_3@GH nanocomposite and calculated no substantial difference in the XRD pattern of the Sn-Gd_2O_3 nanomaterial sample, except a decrease in the intensity of the peaks. No significant peaks were observed for the dopant due to its low concentration.

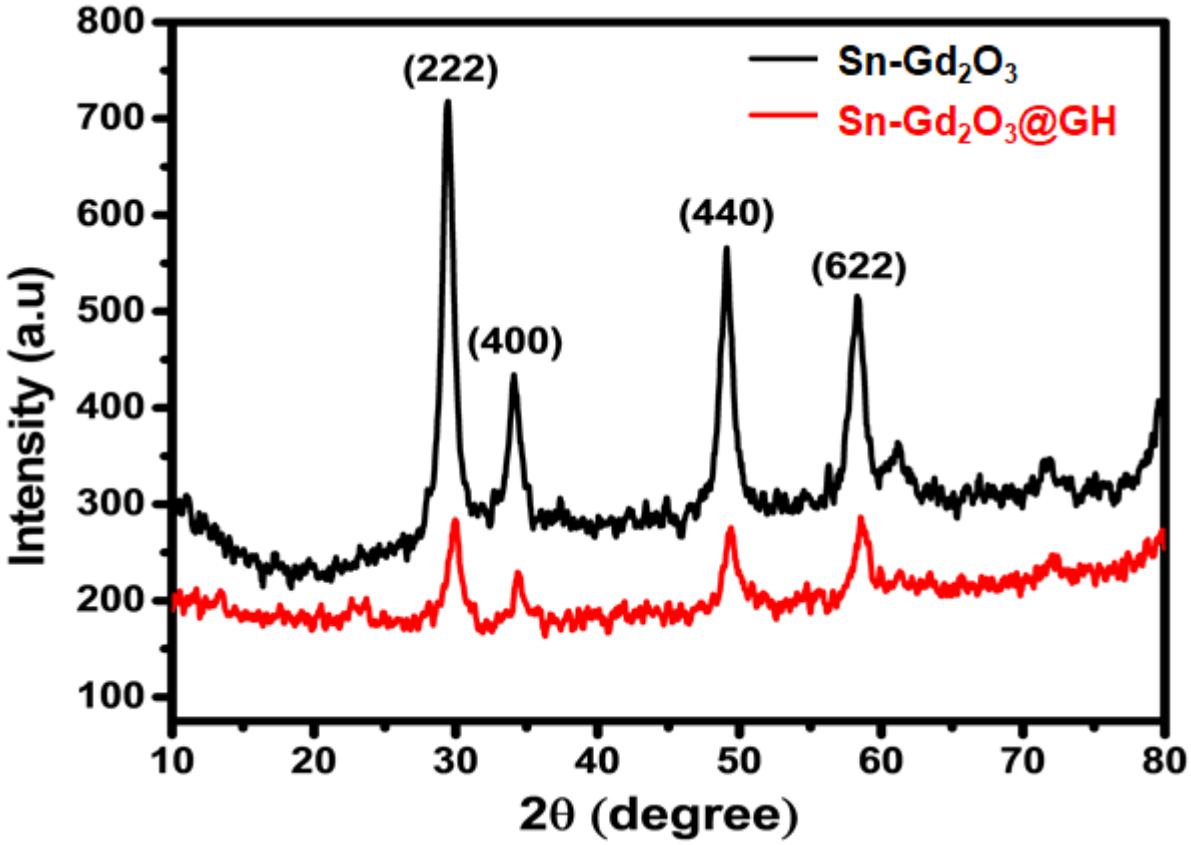

Figure 4. XRD patterns of Sn-Gd_2O_3 nanomaterial (Black-line) and Sn-Gd_2O_3@GH nanocomposite (Red-line).

3.4. FTIR Analysis

FTIR is used to investigate the chemical composition of the sample surface, examine the different functional groups residing in the molecular structure of the compound, and identify peaks change in the mixed substances. Herein, the spectra were systematically recorded in the range of 500–4000 cm^{-1} for the sample analysis. Figure 5 shows the ATR–FTIR spectra of Sn-Gd_2O_3, and dried Sn-Gd_2O_3@GH nanocomposite film. In the FTIR spectrum of powder Sn-Gd_2O_3, the characteristic peaks at 1643, 1513, and 1379 are attributed to the –OH vibration of water and asymmetric stretching vibrations of the carbonate group which may be due to the presence of the air [62], the two prominent peaks exhibited at 3322 and 618 cm^{-1} that are related to the symmetric stretching vibration of –OH, and the Gd=O vibrational band of Sn-Gd_2O_3. Similarly, many peaks appeared in the FTIR spectra of Sn-Gd_2O_3@GH nanocomposite. The peaks observed at 3284 and 2930 cm^{-1} were attributed to the stretching of N–H functional and C–H stretching vibration of gelatin

structure. The peak at 1636 cm^{-1} is present amid I; the peak at 1409 cm^{-1} is attributed to the C–H bending vibration; while peaks appearing at 1438 and 1537 cm^{-1} suggest C–H aliphatic vibration and asymmetric stretching vibration of carboxyl group, respectively. Similarly, the peak which appeared at 1337 is attributed to the N–H stretching vibration. Moreover, the broader peak was appeared for Gd=O, at 553 cm^{-1}, which is similar to published report [63], and confirm the presence of a Sn-Gd_2O_3nanomaterial in the hydrogel nanocomposite. In FTIR spectrum of powder Sn-Gd_2O_3, the characteristics peaks at 1643, 1513, and 1379 are attributed the stretching vibration of hydroxyl and asymmetric stretching vibrations of carbonate group, which may be due to the presence of the air.

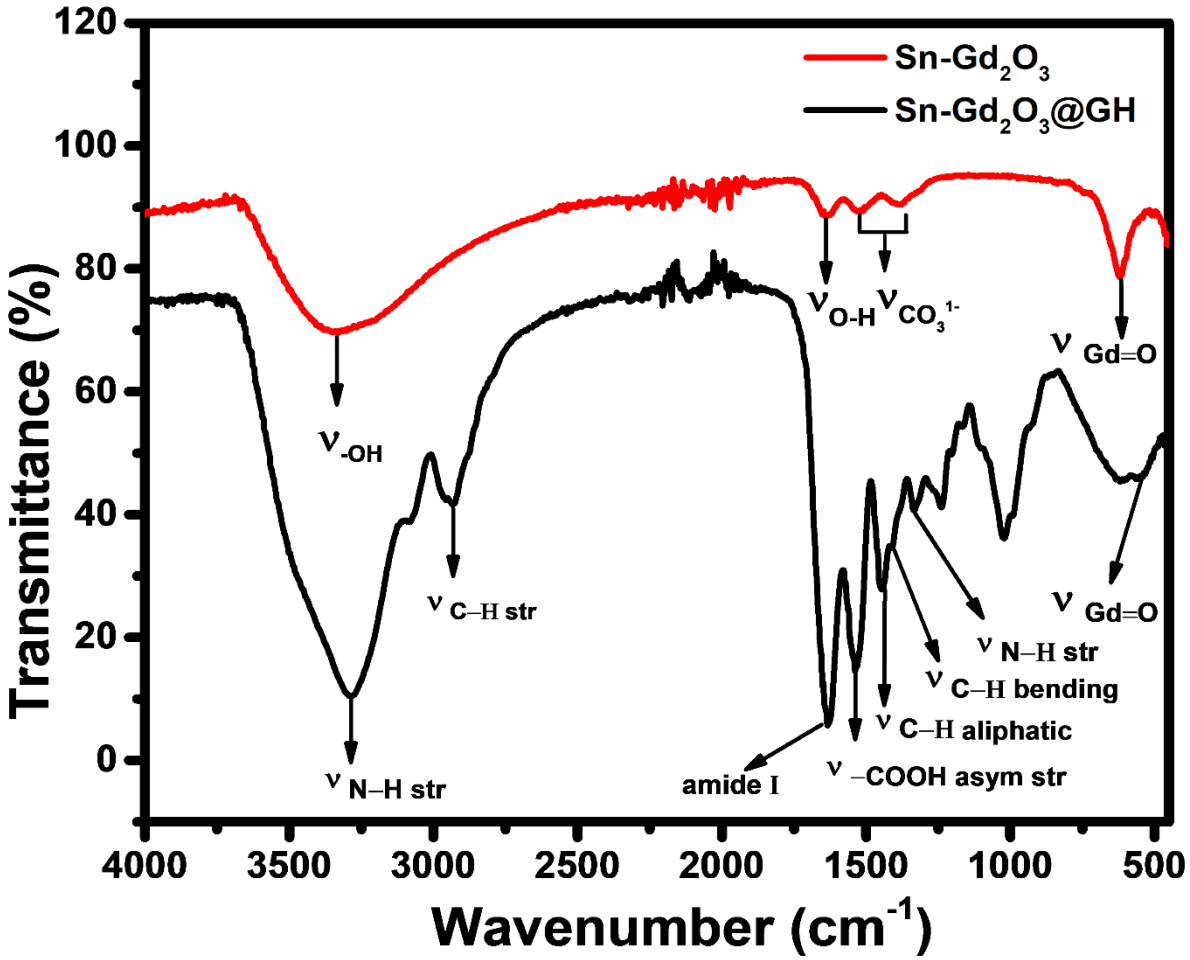

Figure 5. FTIR spectra of Sn-Gd_2O_3 nanomaterial and Sn-Gd_2O_3@GH nanocomposite.

4. Result and Discussion

4.1. Dyes Reduction

The catalytic activity of Sn-Gd_2O_3 NPs was analysed against two series of different dyes, such as azo dyes, and different NPs. For each dye, 25 mL of (0.07 mM) of each MB, MO, and CR were added into a 50 mL beaker with strong reducing agent $NaBH_4$ under constant stirring. The reduction of the dyes was investigated by introducing 0.4 g of $NaBH_4$, which suddenly brought a small change in the colour of the dyes. A catalyst of 0.2 gm (Sn-Gd_2O_3@GH) was added to the beaker promptly after adding the $NaBH_4$. The catalytic reduction was recorded through UV–visible spectrometer. For the recording of every spectral line the dye was introduced to quartz cuvette cell of 3.5 mL. For the reduction investigation, tiny amount of the aliquot was taken out in the beaker in quartz cuvette for spectral analysis. The cuvette solution is drained off into the beaker again and continued the process until completion of the reaction. The hydrogel nanocomposite

reduced the MO and CR in 16 and 4 min, respectively. No change in the spectra of MB was observed for 20 min. Similarly, different nitro phenols, such as 4-NP, 2,6-DNP, and 2-NP, were investigated following the same process as discussed above. Hence, the 4-NP, 2,6-DNP, and 2-NP nitrophenols were reduced in 16, 12, and 8 min, respectively.

Therefore, the catalytic efficiency of Sn-Gd_2O_3@GH catalyst reduced the MO, CR, 4-NP, 2,6-DNP, and 2-NP, among which the CR was reduced efficiently in 4 min. The concentration of all of the dyes was 0.07 mM, using 0.4 gm of $NaBH_4$, and 0.2 gm of the catalyst throughout the experiment.

4.1.1. Catalytic Reduction of NPs

The catalytic activity of Sn-Gd_2O_3@GH nanocomposite was investigated against 4-NP, 2,6-DNP, and 2-NP with of strong reducing agent ($NaBH_4$), as model reactions. UV–visible absorption spectra were recorded verses irradiation time to investigate the colour changes in the reaction phase. It was observed that the addition of 0.4 g of strong reducing agent to different nitrophenol solutions caused an immediate change in their colour. However, no decrease in the intensity at main peaks was observed. Upon 0.2g of Sn-Gd_2O_3@GH nanocomposite addition as a catalyst to the solutions, the NPs were reduced. For each reaction, 25 mL of dye solution (0.07 mM) was added to a 50 mL beaker, proceeding with the addition of 0.4 gm $NaBH_4$ and 0.2 gm catalyst under constant stirring.

Figure 6a shows the catalytic reduction of 4-NP to (4-aminophenol) 4-AP with reducing agent $NaBH_4$. The aqueous solution of 4-NP showed a maximum absorption peak (λ_{max}) at 317 nm, which red shifted to 398 nm, with the addition of $NaBH_4$. This shift confirms the formation of 4-nitropnolate ions as described in some previous reports [64,65]. Due to the addition of 0.2g hydrogel catalyst, the intensity of the peak at 398 nm starts decreasing with the concomitant increase in 4-AP peak at 300 nm. Therefore, the light yellow solution of 4-NP had disappeared after 16 min. A similar procedure was followed for the 2,6-DNP and 2-NP (0.07 mM), as shown in (Figure 6b,c).

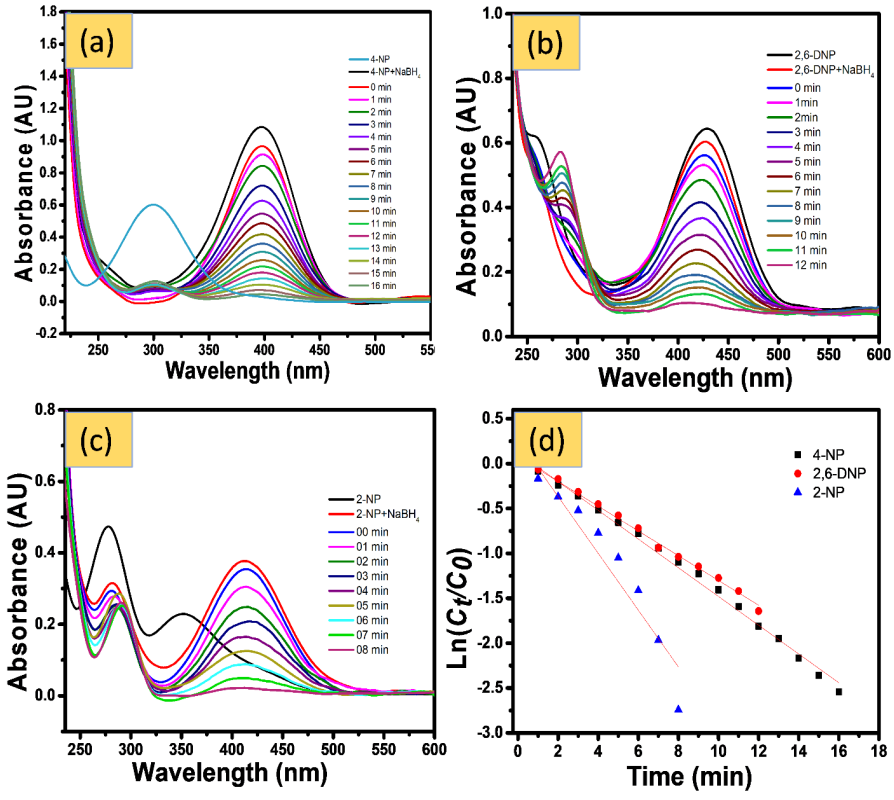

Figure 6. Typical UV−visible absorbance spectra of 4−NP (**a**), 2,6−DNP (**b**), and 2−NP (**c**) and their (**d**) Ln(At/A0) vs. time plot for the reduction reactions where the amount of the Sn-Gd_2O_3@GH catalyst was 0.2 g.

Their peaks appeared at 428 nm and 413 nm were reduced in 12 and 8 min, respectively. In these catalytic reactions, the concentration of $NaBH_4$ was much higher and can be considered constant. Kinetic study was proposed to investigate the mechanism of adsorption process of the dye on the contact surface of the catalyst. To quantitatively measure the rate of these redox reactions, the UV–vis spectral data was calculated through the following pseudo-first-order kinetics.

$$\text{Ln}\ (C_t/C_0) = \text{Ln}(A_t/A_0) = -K_{app}\ \text{t} \quad (1)$$

where C_0 is the initial concentration of the dye and C_t is the concentration of the dye at any given interval of time. A_0 and A_t are the absorbance value take before and after introducing $NaBH_4$, respectively, and catalysts to the reaction media. K_{app} represent the apparent rate constant, while t represents the rate of the reaction.

Therefore, the catalytic efficiency of Sn-Gd_2O_3@GH catalyst on the reduction of 4-NP, 2,6-DNP, and 2-NP can be described as pseudo first-order. The reduction rates of 4-NP, 2,6-DNP and 2-NP were reported as 1.6×10^{-1}, 1.4×10^{-1}, and 1.8×10^{-1} min^{-1}, respectively.

4.1.2. Catalytic Reduction of Azo Dyes

In this approach, the reduction of different dyes, such as CR, 4-MO, and MB was also examined using $NaBH_4$ in the presence of Sn-Gd_2O_3@GH catalyst. All dyes of the same concentration of (0.07 mM), were investigated following the same process as above. Figure 7 showed that CR and MO dyes were reduced within 4 and 16 min by $NaBH_4$ (in presence of Sn-Gd_2O_3@GH) in one min interval at room temperature, except MB which was investigated for 18 min showing no progress in reduction. The corresponding rate of reduction of the CR and MO was reported as 0.842 and 0.197 min^{-1}, respectively. The reduction rate was linearly associated with Equation (1). Therefore, the catalytic reduction with $NaBH_4$ (In presence of Sn-Gd_2O_3@GH catalyst) was reported efficient for CR dye.

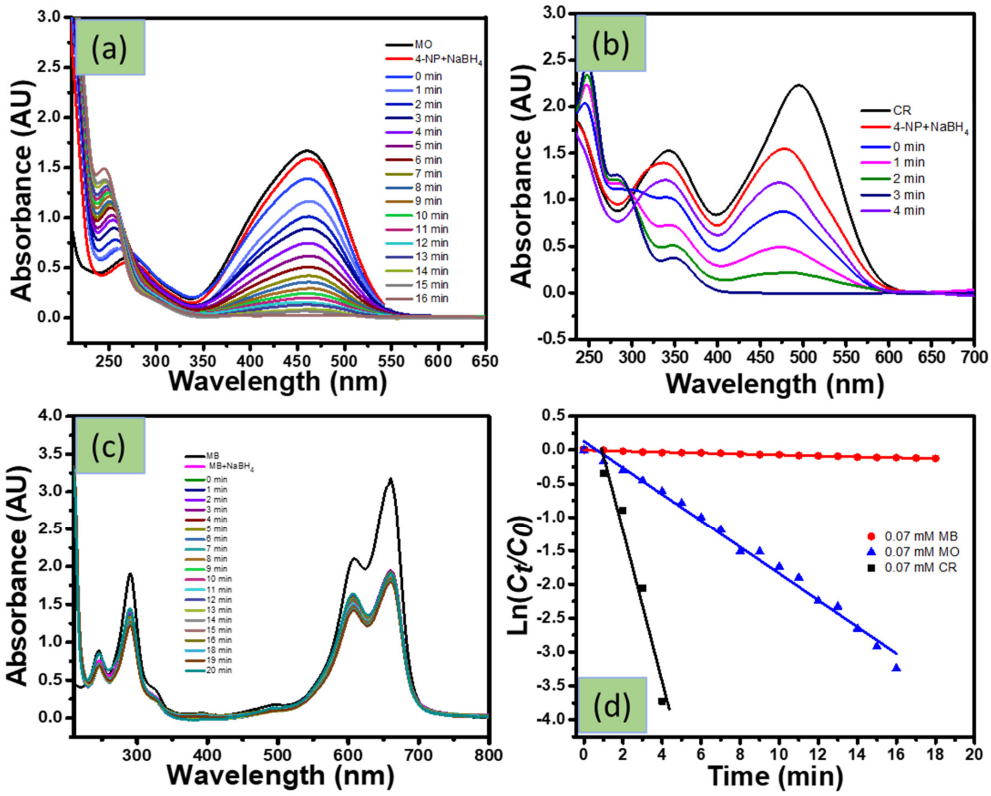

Figure 7. Typical UV–visible absorbance spectra of 4-MO (**a**), CR (**b**), and MB (**c**) and their and Ln(At/A0) vs. time plot (**d**) for the reduction reactions with $NaBH_4$/Sn-Gd_2O_3@GH. The amount of the Sn-Gd_2O_3@GH catalyst was kept fixed (0.2 g).

4.1.3. Catalytic Reduction Changing Experimental Parameter

The industrial development causes a serious threat to human beings owing to the release of huge number of pollutants, especially dyes, to direct stream flow. These dyes' molecules contain double bond azo group (–N=N–) in their skeleton of chemical structure [66,67]. Synthetic dyes are used for various purposes, mainly in the cosmetic, food, pulp, paper, and textile industries. In particular, CR and MO are both anionic azo dyes, which are used as indicators as well as in the food, textile, paper and pulp, cotton, silk, plastic, cosmetic, pharmaceutical, rubber, printing, and wool industries [68]. Despite the useful applications of CR, it also causes eye and skin irritation, gastro-intestinal irritation, and vomiting, while its long-term subjection to the body causes liver tumours in women [69]. CR dye is also used as a biological stain in medicine for diagnosis of amyloidosis and an indicator in acidic media [70,71].

Therefore, the catalytic reduction of CR dye was carried out with strong reducing agent ($NaBH_4$) and Sn-Gd_2O_3@GH, with Sn-Gd_2O_3@GH nanocomposite as the catalyst. For the spectral reduction of CR dye in the presence of $NaBH_4$/Sn-Gd_2O_3@GH, the UV–visible spectrometer was found and presented in Figure 8a.

The UV–Vis spectrum of reduction of CR was recorded for 4 min in the presence of $NaBH_4$, using 0.2 gm of Sn-Gd_2O_3@GH catalyst (Figure 8a). With the introduction of $NaBH_4$ to the aqueous medium of CR, the absorption peak at 495 nm was reduced to absorption band (λ_{max}) at 475 nm.

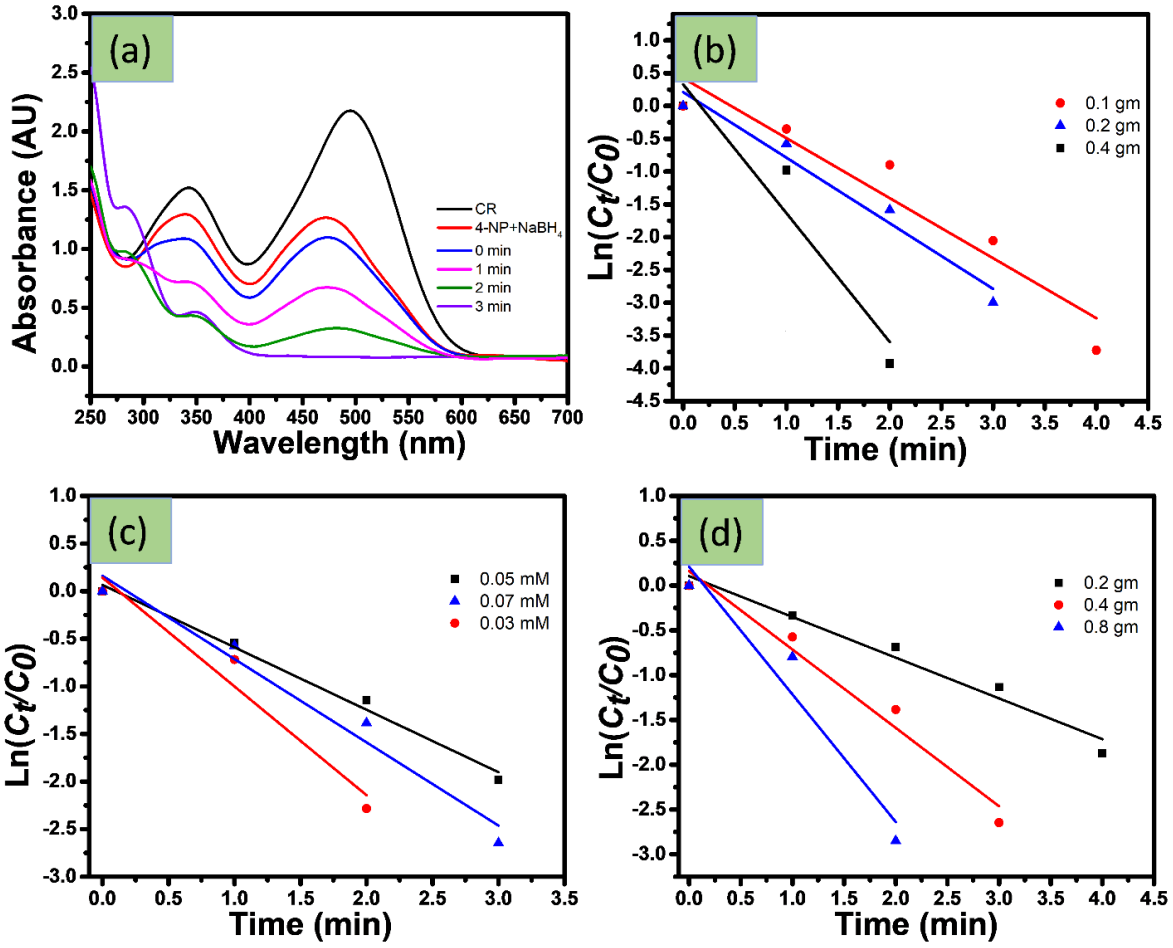

Figure 8. UV–visible spectra of CR dye reduction with $NaBH_4$/Sn-Gd_2O_3@GH (**a**). Optimization of CR dye degradation. The plot of ln (Ct/C0) versus time for CR dye by changing amount of Sn-Gd_2O_3@GH catalyst (**b**). Different concentrations of CR dye (**c**) and changing the amount of NaBH4 (**d**).

In the reaction mixture of CR+$NaBH_4$, the concentration of $NaBH_4$ was kept higher, which resulted in the increase in the pH of the reaction mixture. The addition of hydrogel nanocomposite (Sn-Gd_2O_3@GH catalyst) helps in catalytic reduction by transferring electrons from electron donor species BH_4^- to electron acceptor species CR. The catalyst decreases the activation energy and stabilize the reaction mixture [72]. As the reaction mixture is independent on the concentration of the $NaBH_4$, and hence, for the catalytic reduction of the present mixture a pseudo first order kinetics could be used. Therefore, the linear relationship between $\ln(C_t/C_0)$ (where A_0 is absorbance of the initial concentration, A_t is the absorbance at the specific reaction time) vs. time confirmed that the reaction is of the pseudo-first order. Further, the efficiency of Sn-Gd_2O_3@GH was further optimized and analysed against different catalyst amounts (Sn-Gd_2O_3@GH), $NaBH_4$ amounts, and CR concentrations.

The change in reduction rate was further analysed, changing 0.1, 0.2, and 0.4 gm of Sn-Gd_2O_3@GH catalyst against CR, in the presence of 0.4 gm $NaBH_4$. The UV–vis absorbance was recorded in 1 min intervals. For each run, 25.0 mL (0.07 mM) CR was introduced into the beaker, followed by the addition of 0.4 gm $NaBH_4$, adding 0.1, 0.2, or 0.4 gm catalyst, respectively. That widely records the decrease in reduction time of the dye by increasing catalyst amount. The reduction of the CR was complete in 4, 3, and 2 min with the reduction rate of 0.915, 0.999, and 1.96 min^{-1}, respectively. This clearly demonstrates that the reduction time decreases with the increase in the catalyst amount, as 0.4g of Sn-Gd_2O_3@GH reduced the CR in 2 min with reduction rate of 1.96 min^{-1}, as shown in Figure 8b. To determine the catalyst efficiency against different concentrations of the dye, three different concentrations, 0.07, 0.05, and 0.03 mM of the CR dye were prepared. Each concentration of 25.0 mL was consecutively introduced into a 50.0 mL beaker using 0.4 gm of $NaBH_4$ and 0.2g of the prepared catalyst. The CR was reduced in 3, 3, and 2 min with a corresponding rate of 0.875, 0.656, and 1.14 min^{-1}, respectively. The 0.03 mM was reduced with high reduction rate of 1.14 min^{-1} as shown in Figure 8c. Similarly, Figure 8d represents the effect of $NaBH_4$ for the reduction of 0.07 mM CR. Herein, three different weights of 0.2, 0.4, and 0.8 gm of $NaBH_4$ were added to 25 mL of the (0.07 mM) dye using 0.2 gm of the catalyst. By the transfer of the above $NaBH_4$ amount to the beaker in the presence of catalyst, the dye was reduced in 4, 3, and 3 min with reduction rate of 0.455, 0.875, and 1.42 min^{-1}, respectively. Again, the higher reduction rate of 1.42 min^{-1} confirmed the influence of $NaBH_4$ on the catalytic efficiency of Sn-Gd_2O_3@GH nanocomposite. The apparent rate constant (K_{app}) of the pseudo order kinetic for all changing parameters is shown in (Figure 8b–d) between $\ln(C_t/C_0)$ and time, which were fitted with the above linear Equation (1). Similarly, the % reduction in the dyes was calculated using the given Equation (2).

$$\text{Reduction (\%) } C/C_0 = [(A_0 - A_t)/A_0] * 100 \quad (2)$$

where A_0 and A_t are corresponding to the initial absorbance of the dye and absorbance at time '*t*', respectively.

5. Mechanism of Reduction

CR is a di-azo dye widely used in different industries. Besides its importance, it is also hazardous to nature. Therefore, from an environmental point of view, its reduction is absolutely paramount. Its chemical structure is composed of two phenyl groups which are connected by two diazo binding to the two naphthalene on the both side of the biphenyl group [73]. Reduction of CR molecules cannot be carried out by $NaBH_4$ because this reaction is not feasible kinetically. Therefore, here, the reduction of CR is carried out by Sn-Gd_2O_3@GH nanocomposite with $NaBH_4$. Figure 9 shows the reduction of CR, which is converted into its corresponding constituents. Before introducing the catalyst to the reaction media, a high concentration of $NaBH_4$ was employed to the aqueous solution of CR, which raised the pH of the solution and changed its colour from dark red to lighter red. The $NaBH_4$ gives BH_4^- and acts as an electron donor. By introducing the Sn-Gd_2O_3@GH catalyst, the BH_4^- and dye molecules adsorb on the surface of the catalyst. The surface of

the nanomaterial acts as mediator for transferring electrons from borohydride ions (BH_4^-) to CR molecules. The catalyst provides an efficient pathway to transfer electrons to CR molecules and reduced it in a small amount of time. Finally, the CR molecule was broken down into 1,1′-bipheny, sodium(4-amino-naphthalene)-1-sulfonate, and nitrogen.

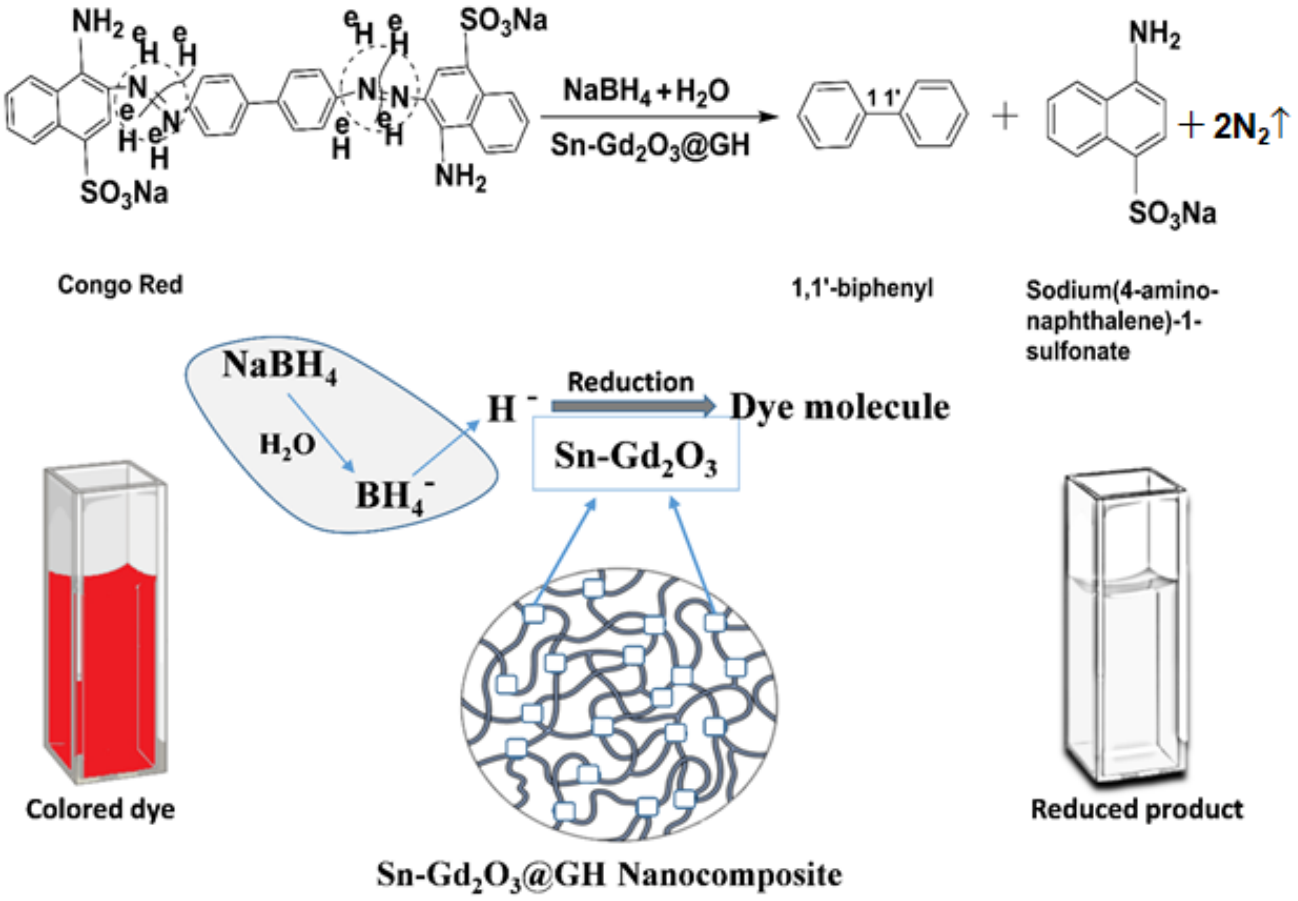

Figure 9. Scheme for the reduction of the CR by NaBH4 using Sn-Gd_2O_3@GH hydrogel catalyst.

6. Reusability of Catalyst

Here, the important factor of the efficient catalyst is its recyclability property [74]. The recyclability determines the durability and performance of the catalyst. Here, the Sn-Gd_2O_3@GH catalyst was checked for three cycles after successful completion of the reaction. Figure 10 exhibits the C/C_0 (%) and k_{app} of three catalytic reduction reactions of CR dye. The catalyst was easily recovered from the reaction mixture simply by filtration and then washed with distilled water and reused again.

It is clearly observed form Figure 10 that CR was reduced by Sn-Gd_2O_3@GH with sodium borohydrate in 4, 5, and 5 min, respectively, up to 97.6, 89.7, and 85.8 %, with catalytic rate of 9.15×10^{-1}, 5.67×10^{-1}, and 3.98×10^{-1} min^{-1}, respectively. The concentration of $NaBH_4$ was kept constant throughout the recyclability. For each cycle, the recovered amount of Sn-Gd_2O_3@GH hydrogel catalyst was used against 0.7 mM solution of CR. A slight decrease was exhibited in the activity of the catalyst with reusability.

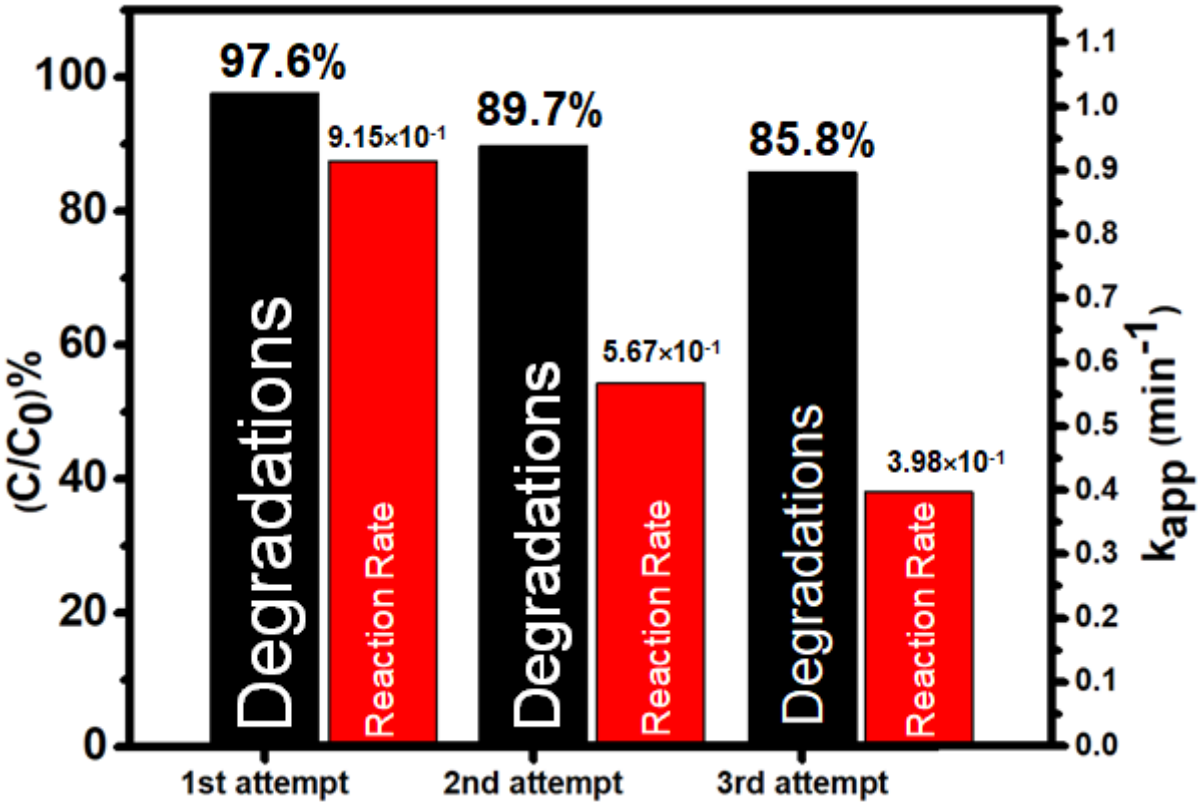

Figure 10. Recyclability of the Sn-Gd_2O_3@GH hydrogel catalyst. Degradation (red) and reaction rate (black) histograms are shown for the reusability of Sn-Gd_2O_3@GH catalyst during CR degradation in the presence of borohydrate.

7. Conclusions

Sn doped Gd_2O_3 nanomaterial was successfully prepared. The nanomaterial was simply prepared by mixing of 0.1 M solution of $Gd[NO_3]_3{\cdot}6H_2O$ and $SnCl_4$ at PH > 10. The solution was heated in a Teflon-lined autoclave at 150 °C to obtain the white precipitate of the sample. Then, 0.4 % by weight of the white precipitate of Sn-Gd_2O_3 was treated with 20 mL of gelatin solution and cross-linked with formaldehyde, and finally Sn-Gd_2O_3@GH nanocomposite was synthesized. The hydrogel nanocomposite was further used as a catalyst against different dyes, such as 4-NP, 2,6-DNP, 2-NP, MB, MO, and CR, in the presence of strong reducing agent $NaBH_4$. The Sn-Gd_2O_3@GH catalyst reduced the CR efficiently with respect to other dyes, with a 9.15×10^{-1} min^{-1} rate of reaction. The XRD pattern confirms the tetragonal rutile phase of the crystal. The SEM micrographs evaluate the average crystalline size of Sn-Gd_2O_3nanomaterial, which is calculated as 30.06 nm, while EDS peaks confirm the incorporated material in the hydrogel nanocomposite. Therefore, the present approach leads to the fabrication of a new hydrogel nanocomposite for the removal of water pollutants, which is efficient for the reduction activity of dyes and can be easily recycled and reused.

Author Contributions: Conceptualization, H.M.M. and S.A.; methodology, S.A.; software, S.A.; validation, S.A., H.M.M. and M.M.R.; formal analysis, S.A.; investigation, S.A.; resources, H.M.M.; data curation, S.A. and M.M.R.; writing—original draft preparation, S.A. and H.M.M.; writing—review and editing, M.M.R.; visualization, H.M.M. and M.M.R.; supervision, H.M.M.; project administration, H.M.M.; funding acquisition, H.M.M. All authors have read and agreed to the published version of the manuscript.

Funding: This work was funded by the Deanship of Scientific Research (DSR), King Abdulaziz University, Jeddah, under grant No. D-031-130-1443.

Institutional Review Board Statement: Not applicable.

Informed Consent Statement: Not applicable.

Data Availability Statement: Data will be available upon reasonable request.

Acknowledgments: This work was funded by the Deanship of Scientific Research (DSR), King Abdulaziz University, Jeddah, under grant No. D-031-130-1443. The authors, therefore, acknowledge with thanks DSR technical and financial support.

Conflicts of Interest: The authors declare that they have no conflict of interest.

References

1. Phipps, G.L.; Holcombe, G.W.; Fiandt, J.T. Acute toxicity of phenol and substituted phenols to the fathead minnow. *Bull. Environ. Contam. Toxicol.* **1981**, *26*, 585–593. [CrossRef]
2. Fakhru'l-Razi, A.; Pendashteh, A.; Abdullah, L.C.; Biak, D.R.A.; Madaeni, S.S.; Abidin, Z.Z. Review of technologies for oil and gas produced water treatment. *J. Hazard. Mater.* **2009**, *170*, 530–551. [CrossRef]
3. Ali, N.; Azeem, S.; Khan, A.; Khan, H.; Kamal, T.; Asiri, A.M. Experimental studies on removal of arsenites from industrial effluents using tridodecylamine supported liquid membrane. *Environ. Sci Pollut. Res.* **2020**, *27*, 11932–11943. [CrossRef]
4. Devi, L.G.; Kumar, S.G.; Reddy, K.M.; Munikrishnappa, C. Photo degradation of Methyl Orange an azo dye by Advanced Fenton Process using zero valent metallic iron: Influence of various reaction parameters and its degradation mechanism. *J. Hazard. Mater.* **2009**, *164*, 459–467. [CrossRef]
5. Robinson, T.; McMullan, G.; Marchant, R.; Nigam, P. Remediation of dyes in textile effluent: A critical review on current treatment technologies with a proposed alternative. *Bioresour. Technol.* **2001**, *77*, 247–255. [CrossRef]
6. Kamal, T.; Khan, S.B.; Asiri, A.M. Nickel nanoparticles-chitosan composite coated cellulose filter paper: An efficient and easily recoverable dip-catalyst for pollutants degradation. *Environ. Pollut.* **2016**, *218*, 625–633. [CrossRef]
7. Haider, S.; Kamal, T.; Khan, S.B.; Omer, M.; Haider, A.; Khan, F.U.; Asiri, A.M. Natural polymers supported copper nanoparticles for pollutants degradation. *Appl. Surf. Sci.* **2016**, *387*, 1154–1161. [CrossRef]
8. Ahmad, I.; Khan, S.B.; Kamal, T.; Asiri, A.M. Visible light activated degradation of organic pollutants using zinc-iron selenide. *J. Mol. Liq.* **2017**, *229*, 429–435. [CrossRef]
9. Kamal, T.; Ahmad, I.; Khan, S.B.; Ul-Islam, M.; Asiri, A.M. Microwave Assisted Synthesis and Carboxymethyl Cellulose Stabilized Copper Nanoparticles on Bacterial Cellulose Nanofibers Support for Pollutants Degradation. *J. Polym. Environ.* **2019**, *27*, 2867–2877. [CrossRef]
10. Ahmad, I.; Kamal, T.; Khan, S.B.; Asiri, A.M. An efficient and easily retrievable dip catalyst based on silver nanoparticles/chitosan-coated cellulose filter paper. *Cellulose* **2016**, *23*, 3577–3588. [CrossRef]
11. Kamal, T.; Ahmad, I.; Khan, S.B.; Asiri, A.M. Synthesis and catalytic properties of silver nanoparticles supported on porous cellulose acetate sheets and wet-spun fibers. *Carbohydr. Polym.* **2017**, *157*, 294–302. [CrossRef] [PubMed]
12. Khan, M.S.J.; Khan, S.B.; Kamal, T.; Asiri, A.M. Agarose biopolymer coating on polyurethane sponge as host for catalytic silver metal nanoparticles. *Polym. Test.* **2019**, *78*, 105983. [CrossRef]
13. Ali, N.; Ismail, M.; Khan, A.; Khan, H.; Haider, S.; Kamal, T. Spectrophotometric methods for the determination of urea in real samples using silver nanoparticles by standard addition and 2nd order derivative methods. *Spectroc. Acta Part A Molec. Biomolec. Spectr.* **2018**, *189*, 110–115. [CrossRef] [PubMed]
14. Kamal, T.; Ali, N.; Naseem, A.A.; Khan, S.B.; Asiri, A.M. Polymer Nanocomposite Membranes for Antifouling Nanofiltration. *Recent Pat. Nanotechnol.* **2016**, *10*, 189–201. [CrossRef] [PubMed]
15. Ul-Islam, M.; Ullah, M.W.; Khan, S.; Kamal, T.; Ul-Islam, S.; Shah, N.; Park, J.K. Recent Advancement in Cellulose based Nanocomposite for Addressing Environmental Challenges. *Recent Pat. Nanotechnol.* **2016**, *10*, 169–180. [CrossRef] [PubMed]
16. Ahmed, M.S.; Kamal, T.; Khan, S.A.; Anwar, Y.; Saeed, M.T.; Asiri, A.M.; Khan, S.B. Assessment of Anti-bacterial Ni-Al/chitosan Composite Spheres for Adsorption Assisted Photo-Degradation of Organic Pollutants. *Curr. Nanosci.* **2016**, *12*, 569–575. [CrossRef]
17. Kamal, T.; Khan, S.B.; Asiri, A.M. Synthesis of zero-valent Cu nanoparticles in the chitosan coating layer on cellulose microfibers: Evaluation of azo dyes catalytic reduction. *Cellulose* **2016**, *23*, 1911–1923. [CrossRef]
18. Khan, S.A.; Khan, S.B.; Kamal, T.; Yasir, M.; Asiri, A.M. Antibacterial nanocomposites based on chitosan/Co-MCM as a selective and efficient adsorbent for organic dyes. *Int. J. Biol. Macromol.* **2016**, *91*, 744–751. [CrossRef]
19. Ali, F.; Khan, S.B.; Kamal, T.; Anwar, Y.; Alamry, K.A.; Asiri, A.M. Anti-bacterial chitosan/zinc phthalocyanine fibers supported metallic and bimetallic nanoparticles for the removal of organic pollutants. *Carbohydr. Polym.* **2017**, *173*, 676–689. [CrossRef]
20. Ali, F.; Khan, S.B.; Kamal, T.; Anwar, Y.; Alamry, K.A.; Asiri, A.M. Bactericidal and catalytic performance of green nanocomposite based on chitosan/carbon black fiber supported monometallic and bimetallic nanoparticles. *Chemosphere* **2017**, *188*, 588–598. [CrossRef]
21. Ali, N.; Awais; Kamal, T.; Ul-Islam, M.; Khan, A.; Shah, S.J.; Zada, A. Chitosan-coated cotton cloth supported copper nanoparticles for toxic dye reduction. *Int. J. Biol. Macromol.* **2018**, *111*, 832–838. [CrossRef]
22. Ali, F.; Khan, S.B.; Kamal, T.; Alamry, K.A.; Asiri, A.M.; Sobahi, T.R.A. Chitosan coated cotton cloth supported zero-valent nanoparticles: Simple but economically viable, efficient and easily retrievable catalysts. *Sci. Rep.* **2017**, *7*, 16957. [CrossRef]

23. Kamal, T.; Ul-Islam, M.; Khan, S.B.; Asiri, A.M. Adsorption and photocatalyst assisted dye removal and bactericidal performance of ZnO/chitosan coating layer. *Int. J. Biol. Macromol.* **2015**, *81*, 584–590. [CrossRef]
24. Khan, S.B.; Khan, S.A.; Marwani, H.M.; Bakhsh, E.M.; Anwar, Y.; Kamal, T.; Asiri, A.M.; Akhtar, K. Anti-bacterial PES-cellulose composite spheres: Dual character toward extraction and catalytic reduction of nitrophenol. *RSC Adv.* **2016**, *6*, 110077–110090. [CrossRef]
25. Khan, S.B.; Ali, F.; Kamal, T.; Anwar, Y.; Asiri, A.M.; Seo, J. CuO embedded chitosan spheres as antibacterial adsorbent for dyes. *Int. J. Biol. Macromol.* **2016**, *88*, 113–119. [CrossRef]
26. Kamal, T.; Anwar, Y.; Khan, S.B.; Chani, M.T.S.; Asiri, A.M. Dye adsorption and bactericidal properties of TiO2/chitosan coating layer. *Carbohydr. Polym.* **2016**, *148*, 153–160. [CrossRef]
27. Kavitha, T.; Haider, S.; Kamal, T.; Ul-Islam, M. Thermal decomposition of metal complex precursor as route to the synthesis of Co_3O_4 nanoparticles: Antibacterial activity and mechanism. *J. Alloys Compd.* **2017**, *704*, 296–302. [CrossRef]
28. Ali, F.; Khan, S.B.; Kamal, T.; Alamry, K.A.; Bakhsh, E.M.; Asiri, A.M.; Sobahi, T.R.A. Synthesis and characterization of metal nanoparticles templated chitosan-SiO2 catalyst for the reduction of nitrophenols and dyes. *Carbohydr. Polym.* **2018**, *192*, 217–230. [CrossRef]
29. Kamal, T. Aminophenols formation from nitrophenols using agar biopolymer hydrogel supported CuO nanoparticles catalyst. *Polym. Test.* **2019**, *77*, 105896. [CrossRef]
30. Khan, F.U.; Asimullah; Khan, S.B.; Kamal, T.; Asiri, A.M.; Khan, I.U.; Akhtar, K. Novel combination of zero-valent Cu and Ag nanoparticles@ cellulose acetate nanocomposite for the reduction of 4-nitro phenol. *Int. J. Biol. Macromol.* **2017**, *102*, 868–877. [CrossRef]
31. Kamal, T.; Ahmad, I.; Khan, S.B.; Asiri, A.M. Agar hydrogel supported metal nanoparticles catalyst for pollutants degradation in water. *Desalin. Water Treat.* **2018**, *136*, 290–298. [CrossRef]
32. Khan, M.S.J.; Khan, S.B.; Kamal, T.; Asiri, A.M. Catalytic Application of Silver Nanoparticles in Chitosan Hydrogel Prepared by a Facile Method. *J. Polym. Environ.* **2020**, *28*, 962–972. [CrossRef]
33. Al-Mubaddel, F.S.; Haider, S.; Aijaz, M.O.; Haider, A.; Kamal, T.; Almasry, W.A.; Javid, M.; Khan, S.U.-D. Preparation of the chitosan/polyacrylonitrile semi-IPN hydrogel via glutaraldehyde vapors for the removal of Rhodamine B dye. *Polym. Bull.* **2017**, *74*, 1535–1551. [CrossRef]
34. Islam, M.T.; Kamal, T.; Shin, T.; Seong, B.; Park, S.-Y. Self-assembly of a liquid crystal ABA triblock copolymer in a nematic liquid crystal solvent. *Polymer* **2014**, *55*, 3995–4002. [CrossRef]
35. Kamal, T.; Ahmad, I.; Khan, S.B.; Asiri, A.M. Bacterial cellulose as support for biopolymer stabilized catalytic cobalt nanoparticles. *Int. J. Biol. Macromol.* **2019**, *135*, 1162–1170. [CrossRef]
36. Klinger, J.M. A historical geography of rare earth elements: From discovery to the atomic age. *Extr. Ind. Soc.* **2015**, *2*, 572–580. [CrossRef]
37. Chu, S. *US Department of Energy "Critical Materials Strategy"*; Technical Report; U.S. Department of Energy: Washington, DC, USA, 2011.
38. Adachi, G.; Imanaka, N. The Binary Rare Earth Oxides. *Chem. Rev.* **1998**, *98*, 1479–1514. [CrossRef]
39. Kaita, S.; Hou, Z.; Nishiura, M.; Doi, Y.; Kurazumi, J.; Horiuchi, A.C.; Wakatsuki, Y. Ultimately Specific 1,4-cis Polymerization of 1,3-Butadiene with a Novel Gadolinium Catalyst. *Macromol. Rapid Commun.* **2003**, *24*, 179–184. [CrossRef]
40. Yang, J.; Li, C.; Cheng, Z.; Zhang, X.; Quan, Z.; Zhang, C.; Lin, J. Size-tailored synthesis and luminescent properties of one-dimensional Gd2O3: Eu3+ nanorods and microrods. *J. Phys. Chem. C* **2007**, *111*, 18148–18154. [CrossRef]
41. Imtiaz, A.; Farrukh, M.A.; Khaleeq-ur-Rahman, M.; Adnan, R. Micelle-assisted synthesis of Al_2O_3 CaO nanocatalyst: Optical properties and their applications in photodegradation of 2, 4, 6-trinitrophenol. *Sci. World J.* **2013**, *2013*, 641420.
42. Farrukh, M.A.; Teck, H.B.; Adnan, R. Surfactant-controlled aqueous synthesis of SnO_2 nanoparticles via the hydrothermal and conventional heating methods. *Turk. J. Chem.* **2010**, *34*, 537–550.
43. Farrukh, M.A.; Tan, P.; Adnan, R. Influence of reaction parameters on the synthesis of surfactant-assisted tin oxide nanoparticles. *Turk. J. Chem.* **2012**, *36*, 303–314.
44. Merino, S.; Martín, C.; Kostarelos, K.; Prato, M.; Vázquez, E. Nanocomposite Hydrogels: 3D Polymer–Nanoparticle Synergies for On-Demand Drug Delivery. *ACS Nano* **2015**, *9*, 4686–4697. [CrossRef] [PubMed]
45. Khan, M.; Lo, I.M.C. A holistic review of hydrogel applications in the adsorptive removal of aqueous pollutants: Recent progress, challenges, and perspectives. *Water Res.* **2016**, *106*, 259–271. [CrossRef] [PubMed]
46. Berger, J.; Reist, M.; Mayer, J.M.; Felt, O.; Peppas, N.A.; Gurny, R. Structure and interactions in covalently and ionically crosslinked chitosan hydrogels for biomedical applications. *Eur. J. Pharm. Biopharm.* **2004**, *57*, 19–34. [CrossRef]
47. Bigi, A.; Cojazzi, G.; Panzavolta, S.; Rubini, K.; Roveri, N. Mechanical and thermal properties of gelatin films at different degrees of glutaraldehyde crosslinking. *Biomaterials* **2001**, *22*, 763–768. [CrossRef]
48. Gupta, P.; Vermani, K.; Garg, S. Hydrogels: From controlled release to pH-responsive drug delivery. *Drug Discov. Today* **2002**, *7*, 569–579. [CrossRef]
49. Pal, K.; Banthia, A.K.; Majumdar, D.K. Preparation and characterization of polyvinyl alcohol-gelatin hydrogel membranes for biomedical applications. *AAPS PharmSciTech* **2007**, *8*, E142–E146. [CrossRef]

50. Madhumathi, K.; Shalumon, K.T.; Rani, V.V.D.; Tamura, H.; Furuike, T.; Selvamurugan, N.; Nair, S.V.; Jayakumar, R. Wet chemical synthesis of chitosan hydrogel–hydroxyapatite composite membranes for tissue engineering applications. *Int. J. Biol. Macromol.* **2009**, *45*, 12–15. [CrossRef]
51. Kim, U.-J.; Park, J.; Li, C.; Jin, H.-J.; Valluzzi, R.; Kaplan, D.L. Structure and Properties of Silk Hydrogels. *Biomacromolecules* **2004**, *5*, 786–792. [CrossRef]
52. Ali, F.; Khan, S.B.; Kamal, T.; Alamry, K.A.; Asiri, A.M. Chitosan-titanium oxide fibers supported zero-valent nanoparticles: Highly efficient and easily retrievable catalyst for the removal of organic pollutants. *Sci. Rep.* **2018**, *8*, 6260. [CrossRef] [PubMed]
53. Haider, A.; Haider, S.; Kang, I.-K.; Kumar, A.; Kummara, M.R.; Kamal, T.; Han, S.S. A novel use of cellulose based filter paper containing silver nanoparticles for its potential application as wound dressing agent. *Int. J. Biol. Macromol.* **2018**, *108*, 455–461. [CrossRef] [PubMed]
54. Thakur, S.; Govender, P.P.; Mamo, M.A.; Tamulevicius, S.; Thakur, V.K. Recent progress in gelatin hydrogel nanocomposites for water purification and beyond. *Vacuum* **2017**, *146*, 396–408. [CrossRef]
55. Zhang, T.; Cheng, Q.; Ye, D.; Chang, C. Tunicate cellulose nanocrystals reinforced nanocomposite hydrogels comprised by hybrid cross-linked networks. *Carbohydr. Polym.* **2017**, *169*, 139–148. [CrossRef]
56. Lai, J.-Y. Biocompatibility of chemically cross-linked gelatin hydrogels for ophthalmic use. *J. Mater. Sci. Mater. Med.* **2010**, *21*, 1899–1911. [CrossRef]
57. Karadağ, E.; Kundakcı, S. Application of highly swollen novel biosorbent hydrogels in uptake of uranyl ions from aqueous solutions. *Fibers Polym.* **2015**, *16*, 2165–2176. [CrossRef]
58. Development of a Novel Tissue Adhesive using a Naturally-Derived Small Molecule. Available online: https://apps.dtic.mil/sti/citations/ADA429595 (accessed on 1 June 2003).
59. Buhus, G.; Peptu, C.; Popa, M.; Desbrières, J. Controlled Release of Water Soluble Antibiotics by Carboxymethylcellulose- and Gelatin-based Hydrogels Crosslinked with Epichlorohydrin. *Cellulose Chem. Technol.* **2009**, *43*, 141–151.
60. Zhang, X.; Do, M.D.; Casey, P.; Sulistio, A.; Qiao, G.G.; Lundin, L.; Lillford, P.; Kosaraju, S. Chemical Cross-Linking Gelatin with Natural Phenolic Compounds as Studied by High-Resolution NMR Spectroscopy. *Biomacromolecules* **2010**, *11*, 1125–1132. [CrossRef]
61. Yi, Z.; Wen, B.; Qian, C.; Wang, H.; Rao, L.; Liu, H.; Zeng, S. Intense Red Upconversion Emission and Shape Controlled Synthesis of Gd_2O_3:Yb/Er Nanocrystals. *Adv. Condens. Matter. Physics.* **2013**, *2013*, 509374. [CrossRef]
62. Aghazadeh, M. Preparation of Gd_2O_3 Ultrafine Nanoparticles by Pulse Electrodeposition Followed by Heat-treatment Method. *J. Ultrafine Grained Nanostruct. Mater.* **2016**, *49*, 80–86.
63. Liu, H.; Liu, J. Hollow mesoporous Gd_2O_3: Eu 3+ spheres with enhanced luminescence and their drug releasing behavior. *RSC Adv.* **2016**, *6*, 99158–99164. [CrossRef]
64. Fu, Y.; Huang, T.; Jia, B.; Zhu, J.; Wang, X. Reduction of nitrophenols to aminophenols under concerted catalysis by Au/g-C3N4 contact system. *Appl. Catal. B Environ.* **2017**, *202*, 430–437. [CrossRef]
65. Jana, S.; Ghosh, S.K.; Nath, S.; Pande, S.; Praharaj, S.; Panigrahi, S.; Basu, S.; Endo, T.; Pal, T. Synthesis of silver nanoshell-coated cationic polystyrene beads: A solid phase catalyst for the reduction of 4-nitrophenol. *Appl. Catal. A Gen.* **2006**, *313*, 41–48. [CrossRef]
66. Agarwal, S.; Tyagi, I.; Gupta, V.K.; Ghaedi, M.; Masoomzade, M.; Ghaedi, A.M.; Mirtamizdoust, B. RETRACTED: Kinetics and thermodynamics of methyl orange adsorption from aqueous solutions—Artificial neural network-particle swarm optimization modeling. *J. Mol. Liq.* **2016**, *218*, 354–362. [CrossRef]
67. Tajbakhsh, M.; Alinezhad, H.; Nasrollahzadeh, M.; Kamali, T.A. Green synthesis of the Ag/HZSM-5 nanocomposite by using Euphorbia heterophylla leaf extract: A recoverable catalyst for reduction of organic dyes. *J. Alloys Compd.* **2016**, *685*, 258–265. [CrossRef]
68. Ismail, M.; Gul, S.; Khan, M.I.; Khan, M.A.; Asiri, A.M.; Khan, S.B. Green synthesis of zerovalent copper nanoparticles for efficient reduction of toxic azo dyes congo red and methyl orange. *Green Process. Synth.* **2019**, *8*, 135–143. [CrossRef]
69. Ilayaraja, M.; Krishnan, N.P.; Kannan, R.S. Adsorption of Rhodamine-B and Congo red dye from Aqueous Solution using Activated Carbon: Kinetics, Isotherms, and Thermodynamics. *IOSR J. Environ. Sci. Toxicol. Food Technol.* **2013**, *5*, 79–89.
70. Dawood, S.; Sen, T.K. Removal of anionic dye Congo red from aqueous solution by raw pine and acid-treated pine cone powder as adsorbent: Equilibrium, thermodynamic, kinetics, mechanism and process design. *Water Res.* **2012**, *46*, 1933–1946. [CrossRef]
71. Chatterjee, S.; Chatterjee, S.; Chatterjee, B.P.; Guha, A.K. Adsorptive removal of congo red, a carcinogenic textile dye by chitosan hydrobeads: Binding mechanism, equilibrium and kinetics. *Colloids Surf. A Physicochem. Eng. Asp.* **2007**, *299*, 146–152. [CrossRef]
72. Indana, M.K.; Gangapuram, B.R.; Dadigala, R.; Bandi, R.; Guttena, V. A novel green synthesis and characterization of silver nanoparticles using gum tragacanth and evaluation of their potential catalytic reduction activities with methylene blue and Congo red dyes. *J. Anal. Sci. Technol.* **2016**, *7*, 19. [CrossRef]
73. Naseem, K.; Farooqi, Z.H.; Begum, R.; Irfan, A. Removal of Congo red dye from aqueous medium by its catalytic reduction using sodium borohydride in the presence of various inorganic nano-catalysts: A review. *J. Clean. Prod.* **2018**, *187*, 296–307. [CrossRef]
74. Khan, M.S.J.; Kamal, T.; Ali, F.; Asiri, A.M.; Khan, S.B. Chitosan-coated polyurethane sponge supported metal nanoparticles for catalytic reduction of organic pollutants. *Int. J. Biol. Macromol.* **2019**, *132*, 772–783. [CrossRef]